

# The Effect of Anisotropic Focusing of Lamb Modes on a Carbon-Epoxy Plain Woven Fabric Composite Plate

Silvio C. G. GRANJA <sup>1</sup>, Ricardo T. HIGUTI <sup>2</sup>, Luis ELVIRA <sup>3</sup>,  
Oscar MARTINEZ GRAULLERA <sup>3</sup>, Alberto IBANEZ <sup>3</sup>

<sup>1</sup> Faculty of Exact and Technological Sciences, University of the State of Mato Grosso; Sinop, Brazil  
Phone: +55 66 3511 2121, Fax: +55 66 3511 2100; e-mail: sggranja@unemat-net.br

<sup>2</sup> Department of Electrical Engineering, Universidade Estadual Paulista; Ilha Solteira, Brazil  
e-mail: tokio@dee.feis.unesp.br

<sup>3</sup> Department of Acoustics and Nondestructive Testing, ITEFI, CSIC; Madrid, Spain  
e-mail: luis.elvira@csic.es, oscar.martinez.graullera@csic.es, alberto.ibanez@csic.es

## Abstract

The medium anisotropy give rise to interesting effects in the physics of wave propagation: the angular dependence of the group velocity, the skew angle between phase and group velocities, and the elastic focusing leading to the concentration of wave energy in determinated directions. All these effects are mode dependent and must be taken into account to choose the adequate propagating mode in NDE or SHM applications. In this article the dispersion curves of phase and group velocities, and the patterns of wave focusing for the A0 and S0 modes are theoretically obtained and verified experimentally. The angular dependence of the group velocity and the effect of the anisotropic elastic focusing is studied in a 1.97 mm-thickness multilayer carbon-epoxy plain woven fabric composite. The time traces are obtained by scanning the plate with the aid of a retro-reflective film stuck to the surface using a laser Doppler vibrometer. A good agreement between the theory and the experimental results was obtained. The Maris factor corresponding to the A0 mode shows smoother angular variation than that of the S0 mode which depends much more on the direction.

**Keywords:** elastic focusing, anisotropic multilayered plates, textile carbon fiber composite

## 1. Introduction

The linear elastic wave propagation in anisotropic media can be described by the Christoffel equation, either in unlimited media with bulk waves, or for guided waves in general. In isotropic media with plate-like geometries, the guided waves can be described as Lamb waves and shear horizontal (SH) waves, taking into account that symmetric and antisymmetric modes are present for each type of wave. In anisotropic media, Lamb and SH waves are generally coupled and they are only uncoupled in the material symmetry axes, when these axes exist. Furthermore, symmetric and antisymmetric modes are only present if there is symmetry in the thickness direction of the plate. The medium anisotropy gives rise interesting effects in the physics of wave propagation: the angular dependence of the group velocity, the skew angle between the phase and group velocities, and the elastic focusing, often named phonon focusing, leading to the concentration of wave energy in determinated directions. All these effects are mode dependent. The anisotropic elastic focusing phenomena have been widely studied by Taylor et al. (1969) [1] with phonons in solids, by Maris (1971) [2] in thermal acoustic waves in crystals, by Philip and Viswanathan (1977) [3] and Kolomenskii and Maznev (1993) [4] in phonon-focusing of surface waves in crystals, by Maznev and Avery (1995) [5] on anisotropic plates, by Chapuis et al. (2010) [6] in Lamb waves in multilayer anisotropic plates and recently by Fu et al. (2013) [7] in phonon focusing in NiAl.

The main contribution of this work is to verify the angular wave propagation effect of elastic focusing on a structural textile laminate, composed of nine layers of carbon-epoxy plain woven fabric composite [0/90/+45/90/0/90/-45/90/0]-T300/F155. The dispersion

curves of phase and group velocities, and patterns of wave focusing, given by the Maris factor, for the A0 and S0 modes, are theoretically obtained. Comparisons between theoretical predictions and experimental results were made for the wave angular pattern and for the elastic focusing.

The fundamentals of the theory of guided wave propagation in anisotropic media, the angular wave group dependence, skew angle and elastic focusing are presented in Section 2. The numerical predictions for phase and group velocities, and for the slowness curve and focusing factor are presented in Section 3. In Section 4, the experimental setup and results are presented and compared to the theoretical predictions. Finally, Section 5 presents the final remarks.

## 2. Fundamentals on the theory and problem formulation

Assuming a linearly elastic, nonviscous, nonpiezoelectric medium, described by the generalized Hooke's law, and the stress-strain relationship in the  $\{x_1, x_2, x_3\}$  Cartesian coordinates

$$\sigma_{ij} = c_{ijkl} \varepsilon_{kl}, \quad \varepsilon_{kl} = \frac{1}{2} \left( \frac{\partial u_k}{\partial x_l} + \frac{\partial u_l}{\partial x_k} \right), \quad i, j, k, l = 1, 2, 3. \quad (1)$$

where  $c_{ijkl}$  is the stiffness tensor,  $u_k$  is the particle displacement and  $\sigma_{kl}$  and  $\varepsilon_{kl}$  are the stress and strain tensors, the three equations of motion

$$\frac{\partial \sigma_{ij}}{\partial x_j} = \rho \frac{\partial^2 u_i}{\partial t^2}, \quad i, j = 1, 2, 3 \quad (2)$$

describe the wave propagation in a medium with general anisotropy. For the particular case of guided waves in a plate like medium, when the plate is considered infinite in the  $x_1$  and  $x_2$  direction and finite in the  $x_3$  direction, with  $d$  thickness, then guided waves propagating in the sagittal plane  $x_1 x_3$  can be represented as plane waves with displacements

$$(u_1, u_2, u_3) = (U_1, U_2, U_3) e^{i\xi(x_1 + \alpha x_3 - ct)}, \quad (3)$$

where  $i = \sqrt{-1}$ ,  $\xi$  and  $\alpha\xi$  are the wave vector components in the  $x_1$  and  $x_3$  directions, respectively;  $c = \omega/k$  is the wave phase velocity in the  $x_1$  direction.

Each composite layer (the laminae) of the laminate is considered to be composed by an epoxy matrix reinforced with plain woven carbon fabric. Here, this fabric has two orthogonal axes of symmetry, congruent to the fibers directions, the warp and the weft directions. Although the warp and the weft do not have perfectly equal elastic characteristics, we consider them as equivalent directions leading to the tetragonal symmetry of the layer, describing the stiffness matrix in the Voigt notation by [8]

$$C'^{(n)} = \begin{bmatrix} C'_{11}^{(n)} & C'_{12}^{(n)} & C'_{13}^{(n)} & 0 & 0 & 0 \\ & C'_{11}^{(n)} & C'_{13}^{(n)} & 0 & 0 & 0 \\ & & C'_{33}^{(n)} & 0 & 0 & 0 \\ & & & C'_{44}^{(n)} & 0 & 0 \\ & \text{sym.} & & & C'_{44}^{(n)} & 0 \\ & & & & & C'_{66}^{(n)} \end{bmatrix}, \quad (4)$$

where the prime,  $C'^{(n)}$ , denotes the stiffness matrix of the  $n$ th layer in the crystallographic axes  $\{x'_1, x'_2, x'_3\}$ . For sake of clarity, the  $x_3$  coordinate origin is coincident with the middle plane of the laminate, i.e., the laminate is limited by  $-d/2 \leq x_3 \leq d/2$ .

With those considerations and expanding  $\sigma_{ij}$  in the stress-strain relation as a function of the displacements  $u_k$ , a system of three coupled differential equations in the displacements, or wave polarizations, is obtained. When the wave vector is parallel to a crystallographic axis, the three equations give a system of coupled equations in  $u_1$  and  $u_3$ , describing Lamb waves, and one equation in  $u_2$ , describing shear horizontal (SH) waves[8].

To solve the system of  $n$  layers, conditions of continuity of strains and stresses at the interfaces between consecutive layers are imposed. These continuity conditions can be modeled as being perfect or imperfect continuity [9] to simulate imperfect contact. For a general laminate with surfaces free of stresses at  $x_3 = \pm d/2$  the additional conditions for guided waves are  $\sigma_{33} = \sigma_{23} = \sigma_{13} = 0$ . Furthermore, if  $C$  is the complete stiffness matrix with the  $n$  stiffness sub-matrices  $C^{(n)}$ , represented in the coordinates  $\{x_1, x_2, x_3\}$ , and if the laminate has a symmetric layup sequence, i.e.,  $C(x_1, x_2, x_3) = C(x_1, x_2, -x_3)$ , then symmetric and antisymmetric wave modes can be obtained from different impositions in the middle plane of the laminate:

$$\{u_3(x_1, x_2, 0), \sigma_{23}(x_1, x_2, 0), \sigma_{13}(x_1, x_2, 0)\} = \{0, 0, 0\} \quad (5)$$

for symmetric modes, and

$$\{u_1(x_1, x_2, 0), u_2(x_1, x_2, 0), \sigma_{33}(x_1, x_2, 0)\} = \{0, 0, 0\} \quad (6)$$

for antisymmetric modes

These continuity and middle plane conditions are represented as a system of coupled matricial equations that can be treated with the global matrix method[10], with the transfer matrix method[8], with the stiffness matrix method[9, 11] or with the Legendre orthogonal polynomial method approach[12]. The distinction amongst these approaches relies fundamentally on the presence—or not—of numerical instabilities as the frequency-thickness product increases to high values. Within this work, moderate values of frequency-thickness products are used and any of the mentioned methods can solve the problem.

The resultant characteristic equation of the laminate is mode dependent and can be represented by a determinantal equation  $\mathcal{F}(\omega, k; \theta) = 0$ , where  $\mathcal{F}(\omega, k; \theta)$  is function of the angular frequency  $\omega = 2\pi f$ , the wave number  $k = 2\pi/\lambda$ , and the propagation direction  $\theta$ . The function  $\mathcal{F}$  is more conveniently written as function of the variables  $d/\lambda$  and  $fd$ , where  $d$  is the plate thickness. The solutions of the characteristic equation provide the set of dispersion curves in the  $(d/\lambda) \times fd$  space and can be represented as dispersion curves of phase velocities in the  $fd \times c_p$  space through a direct transformation where the phase velocity is  $c_p = \omega/k = fd/(d/\lambda)$ .

### 2.1. Group velocity and skew angle

One of the most interesting features that anisotropic media present is the dependence of group velocities with the direction of wave propagation. This can be understood by analyzing the dependence of the stiffness matrix with the propagation direction to provide the elastic behavior of waves, for example, in longitudinal bulk waves the velocity in the  $x_1$  direction is easily calculated as  $c_L = \sqrt{C_{11}/\rho}$ , and the P-wave velocity increases with  $C_{11}$ . The group velocity components  $c_{gx}$  and  $c_{gy}$  can be calculated by

$$\begin{bmatrix} c_{gx} \\ c_{gy} \end{bmatrix} = \begin{bmatrix} \cos \theta & -\sin \theta \\ \sin \theta & \cos \theta \end{bmatrix} \begin{bmatrix} \frac{\partial(fd)}{\partial(d/\lambda)} \\ \frac{1}{(d/\lambda)} \frac{\partial(fd)}{\partial \theta} \end{bmatrix}, \quad (7)$$

where  $f$  is the frequency,  $\lambda = 2\pi/k$  is the wavelength and  $k$  is the wave number of the guided wave propagating at the direction  $\theta$ . From this equation, the group velocity direction,  $\varphi = \arctan(c_{gy}/c_{gx})$ , and the skew angle,  $\theta_s = \varphi - \theta$ , can be determined.

## 2.2. Elastic focusing, phonon focusing or amplitude enhancement

Another relevant feature of the wave propagation in anisotropic media is the *phonon focusing*[7, 4, 3, 1], also named *elastic focusing* or *amplitude enhancement*[2]. The elastic focusing is an effect that concentrates the energy of waves in some specific directions while decreases the energy at others directions. The effect can be understood when the skew angle of the group velocity is made present in the study of the wave propagation. The group velocity is easily visualized to be normal to the surface of the inverse of phase velocity, the slowness surface, defined by the  $\vec{s} = (c_p^{-1}) \vec{k}/k = \vec{k}/\omega$ . It is mode dependent and it is a function of the direction  $\theta$ , of the wave vector and the frequency  $f$ . The focusing factor, derived by Maris through geometrical considerations, determines how much energy of a wave propagating through an anisotropic medium is concentrated in the direction  $\theta$  compared to the case of the isotropic medium. Using the slowness surface,  $s(\theta) = c_p^{-1}(\theta)$ , within a fixed frequency, the Maris factor is easily calculated

$$A = \left| \frac{d\varphi}{d\theta} \right|^{-1} = [s^2 + (ds/d\theta)^2]^{-1/2} |K_s|^{-1}, \quad (8)$$

where  $K_s$  is the slowness surface curvature. This enhancement factor was derived assuming bulk waves where no limit exist for the wave propagation.

Analog investigations on Lamb waves in an anisotropic plate was made by Chapuis et al. [6] showing the focusing factor  $\mathcal{A} = Ak \cos(\theta_s)$ , where the dependence with the wave number,  $k$ , and with  $\cos(\theta_s)$  is present.

## 3. Numerical results

The laminate was modeled as having nine homogeneous layers of textile carbon fiber reinforced polymer (TCFRP), each layer with tetragonal material symmetry, with only six independent parameters of the stiffness matrix and density presented in the Table 1. Each layer is rotated accordingly to the layup  $[0/90/+45/90/0/90/-45/90/0]$  and the transfer matrix method was used to determine the propagation modes.

Table 1: Parameters of the TCFRP T300-F155 (Hexcel Composites).

$C_{11} = C_{22}$ (GPa)	$C_{12}$ (GPa)	$C_{13} = C_{23}$ (GPa)	$C_{33}$ (GPa)	$C_{44} = C_{55}$ (GPa)	$C_{66}$ (GPa)	Mass density ( $10^3\text{kg/m}^3$ )	Layer thickness (mm)
61.69	6.962	8.621	12.36	2.767	12.01	1.56	0.22

The first three symmetric, SH0, S0, S1, and the first three antisymmetric, A0, SH1, A1, propagation modes are presented. Those notations are used due to the fact that, in the the symmetry axes  $0^\circ$ ,  $90^\circ$  and  $\pm 45^\circ$ ,  $\{\text{SH0}, \text{SH1}\}$  are true SH modes, and  $\{\text{S0}, \text{S1}\}$  and  $\{\text{A0}, \text{A1}\}$  are related to Lamb waves having the uncoupled equations as in isotropic media. As a consequence of the layup sequence and the tetragonal symmetry the results are  $90^\circ$  periodic and only computations in the  $[0^\circ; 45^\circ]$  range are necessary to determine

the complete angular behavior of phase velocity dispersion curves, slowness curves, group velocities and focusing patterns.

Figure 1 shows the antisymmetric and symmetric modes for wave propagation at  $0.5^\circ$ ,  $22.5^\circ$  and  $44.5^\circ$ . The  $0.5^\circ$  and  $44.5^\circ$  curves are very close to the behavior of the  $0^\circ$  and  $45^\circ$  dispersion curves, respectively. The A0 mode has little angular variation when compared to the others modes A1, SH, SH0, S0 e S1. The SH0 and S0 symmetric modes have considerable angle variation while maintaining a nearly non-dispersive behavior, i.e., the phase velocity is almost constant for a large range into small frequency-thickness product.

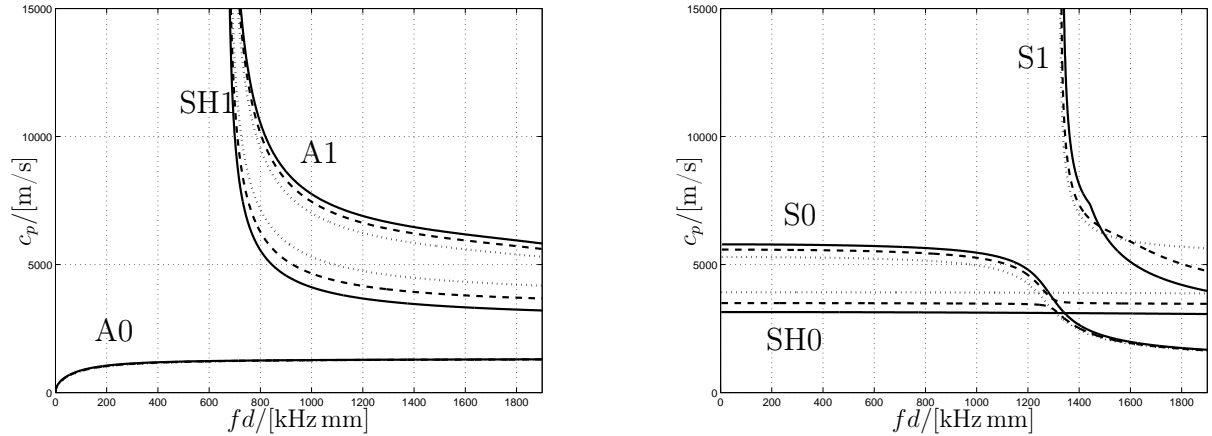


Figure 1: Dispersion curves of phase velocity. Wave propagation at  $0.5^\circ$  (solid curves),  $22.5^\circ$  (dashed curves),  $44.5^\circ$  (dotted curves).

The group velocities for the first three antisymmetric and symmetric modes are shown in Figure 2 and angles  $1^\circ$ ,  $22.5^\circ$  and  $44^\circ$ . The frequency-thickness range  $fd \in [0, 1900]$  kHz mm, corresponding to the frequency range  $f \in [0, 964.46]$  kHz, where  $d = 1.97$  mm.

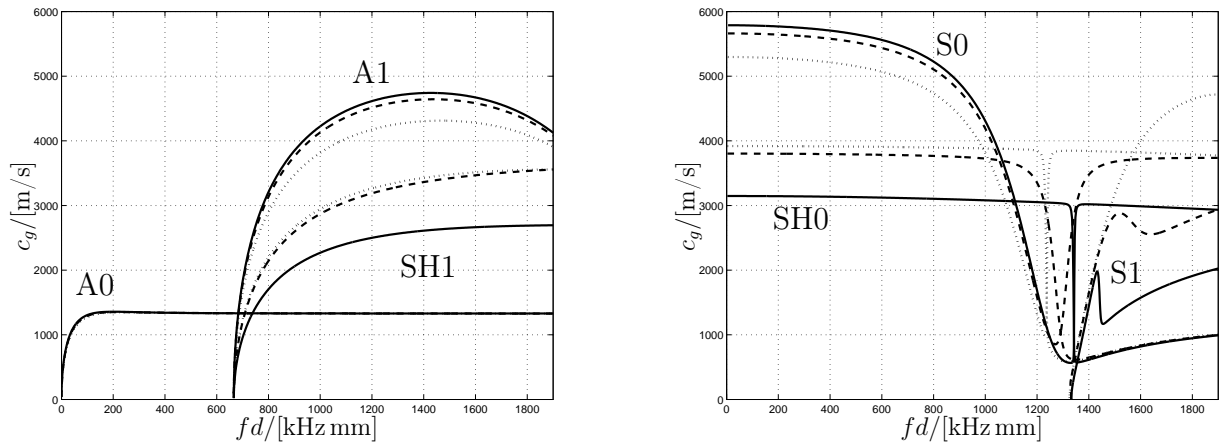


Figure 2: Group velocities dispersion curves. Wave propagation at  $1.0^\circ$  (solid curves),  $22.5^\circ$  (dashed curves),  $44.0^\circ$  (dotted curves).

Figure 3 presents the wave curves for A0 mode at 44 kHz and 310 kHz; and S0 and SH0 modes at 310 kHz. In Figure 3, the A0 mode shows a quasi circular wave curve going from 44 kHz to 310 kHz, with velocities from 1260 m/s to 1335 m/s. The S0 mode shows its anisotropy as a greater angular dependence of the group velocity. The SH0 mode has lower group velocities when compared to the S0 mode, however its curvature suffers fast variations nearby  $45^\circ$ .

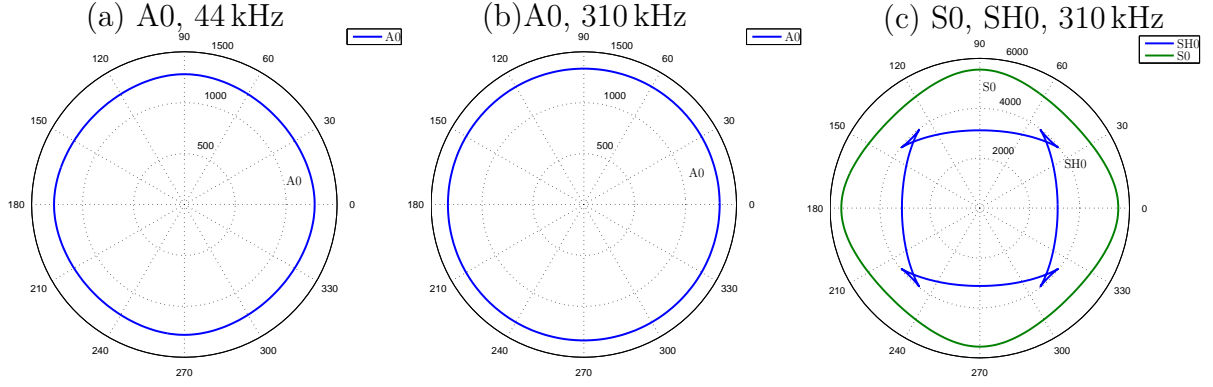


Figure 3: Wave curves for A0 at (a) 44 kHz and (b) 310 kHz; S0 and SH0 at (c) 310 kHz.

The slowness curves  $s(\theta)$  and focusing pattern (Maris factor  $A$ ), of the A0– 44 kHz and 95 kHz– and S0– 310 kHz– modes are presented in Figure 4. These focusing pattern are verified experimentally in the next section.

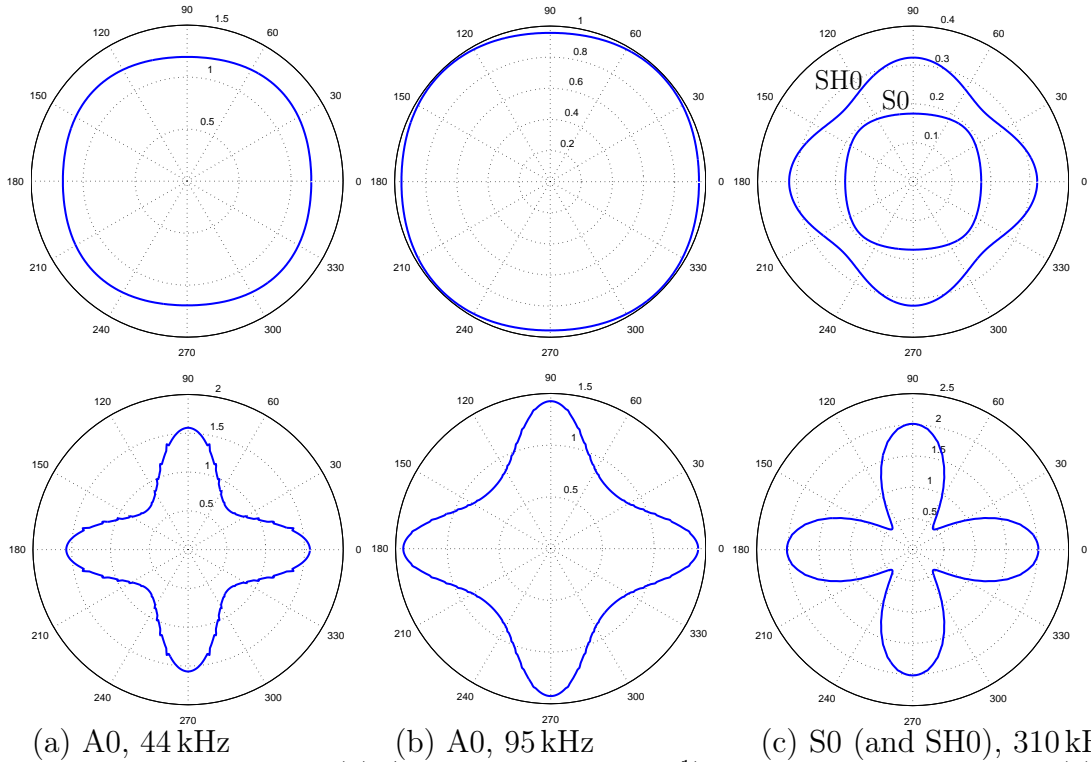


Figure 4: Slowness curves  $s(\theta)$  (on the top, in  $\text{skm}^{-1}$ ) and focusing patterns  $A(\theta)$  (on the bottom, adimensional) for (a) A0 mode at 44 kHz, (b) A0 mode at 95 kHz, and (c) S0 and SH0 modes at 310 kHz.

## 4. Experimental results

An experimental validation was performed using a plain woven carbon-epoxy composite, as described in the numerical results, with nine layers. The experiments were conducted using a PZ-27 ceramic (Ferropem),  $7 \text{ mm} \times 7 \text{ mm} \times 0.5 \text{ mm}$ , glued with cyanoacrylate to the center of the plate and 45 degrees from its principal axis. A signal generator (Agilent, 33120A) was used to apply four cycle tone-burst at 44 kHz and 280 kHz with  $2.0 \text{ V}_{pp}$ , amplified by a 28 dB wide band amplifier (Krohn-Hite, 7602 model) to generate the A0

and S0 modes, respectively. A square retro-reflective film of 21 cm side was glued to the opposite side of the plate, with the ceramic transducer at its center. The time traces were obtained by scanning the retro-reflective film with a laser Doppler vibrometer (Polytec, PSV400) in three scenarios: (1) excitation at 44 kHz and using a 100 kHz low-pass filter; (2) excitation at 280 kHz and bandpass filter from 100 kHz to 500 kHz; and (3) excitation at 600 kHz and 10 kHz high-pass filter.

The A0 and S0 modes have very different group velocities and it was possible to separate them with a window and to perform a spacial analysis of the wave propagation. The A0 maximum response occurs at 44 kHz, 66 kHz and 95 kHz when the transducer is excited at 44 kHz, 280 kHz and 600 kHz. The S0 mode always shows maximum response at 310 kHz. The signals were filtered using Gaussian filters at the maximum response frequencies of each mode. Figures 5, 6 and 7 show a superposition of theoretical and experimental wave curve results for A0 and S0 modes when the transducer is excited at 44 kHz, 280 kHz and 600 kHz, respectively, and with the Gaussian filters applied.

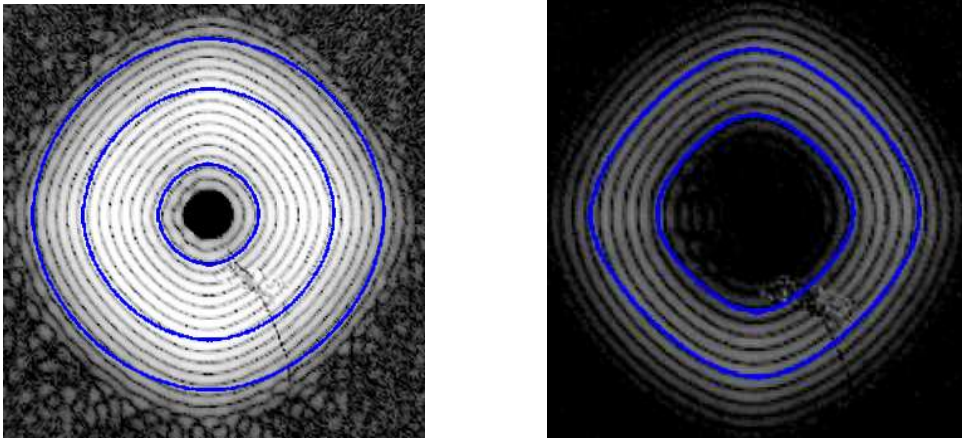


Figure 5: Wave curves for the 1.97 mm-thick laminate with excitation at 44 kHz: prediction in blue and experimental in gray. A0 mode (44 kHz) on the left and S0 mode (310 kHz) on the right.

The predicted wave patterns present a good agreement with the experimental results, although a slight difference between the velocities at  $0^\circ$  and  $90^\circ$  appears. This is probably due to the non-perfect tetragonal symmetry of each layer.

In order to verify the predicted effect of elastic focusing by mathematical modeling the signals previously described were used. The A0 and S0 modes can be separated with a window, as they have remarkable different speeds. Once separated in time, other time and spacial windows were applied to each mode to analyze only a few cycles of the waveform. At this point the maximum amplitude of the wave and its angular dependence were measured. The maximum amplitude is related to the square root of the wave energy and the comparison can be made between the the predicted enhancement of the amplitude,  $\sqrt{A(\theta)}$ , and the angular dependence of the maximum measured amplitude.

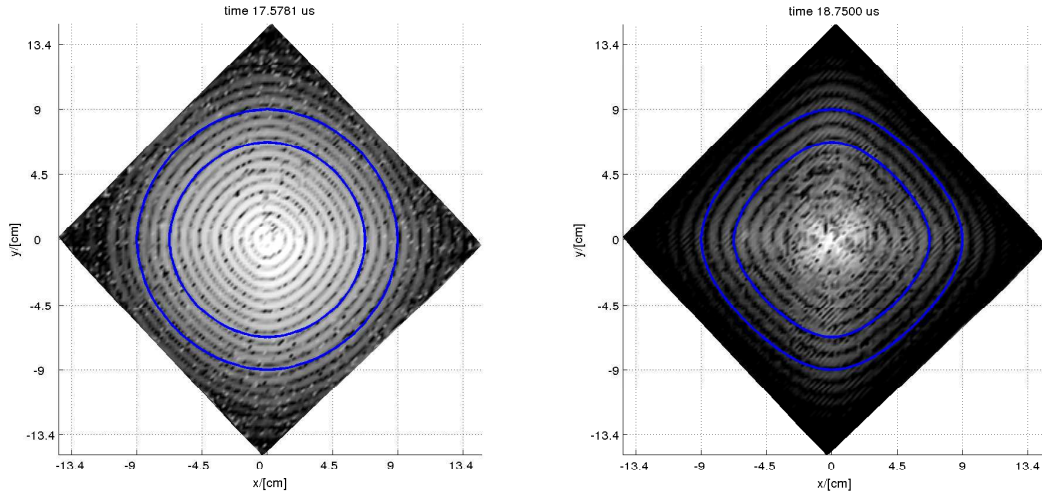


Figure 6: Wave curves for the 1.97 mm-thick laminate with excitation at 280 kHz: prediction in blue and experimental in gray. A0 mode (66 kHz) on the left and S0 mode (310 kHz) on the right.

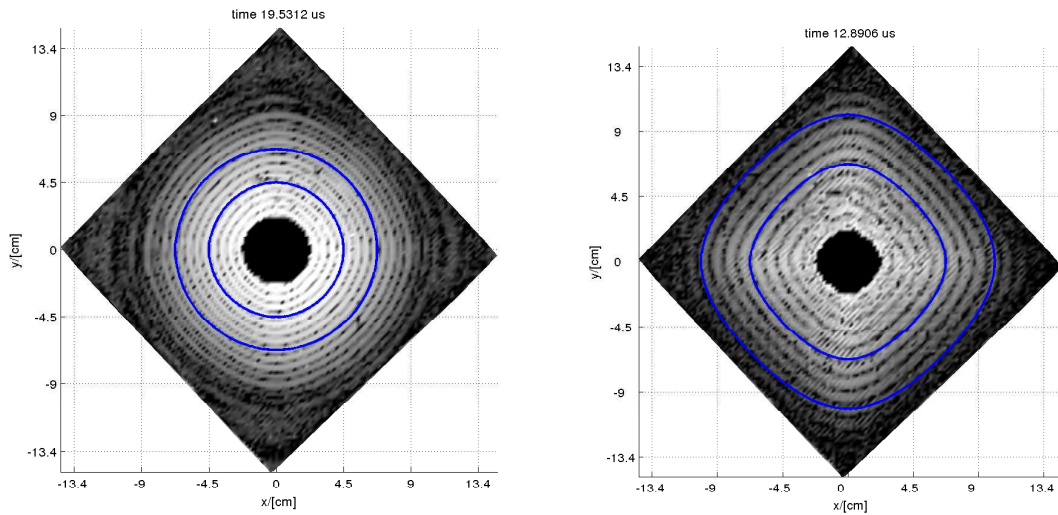


Figure 7: Wave curves for the 1.97 mm-thick laminate with excitation at 600 kHz: prediction in blue and experimental in gray. A0 mode (95 kHz) on the left and S0 mode (310 kHz) on the right.

Figure 8 presents, in linear and polar coordinates, the comparison between theoretical and experimental results of the  $\sqrt{A(\theta)}$  factor, for the A0 and S0 modes with tone-burst excitations at 44 kHz, 280 kHz and 600 kHz, respectively. The fitting of experimental data are best realized in polar coordinates. The three sub-figures were computed using different times of the signals, e.g. the A0 focusing pattern presented is calculated at 165.03 us and the S0 patterns at 23.24 us and 21.8 us, respectively. The pattern of focusing of the A0 mode is only clearly visible with excitation at 44 kHz, while the S0 pattern (not shown here) has a significant amount of noise and cannot be clearly identified. With tone bursts excitations at 280 kHz and 600 kHz, it is the A0 mode which cannot be identified clearly against the background noise, resulting only the S0 mode with a good signal-to-noise ratio.

To compare the experimental results and the theoretical prediction of the elastic focusing, normalization of theoretical curves respect to their maximum angular value was done. Then, a proportionality value was chosen for the experimental data such that the squared error between theory and experiments is minimized. There is a clear difference between the A0 and the S0 mode patterns. The behavior of A0 mode has a smooth angular variation compared to de S0 mode, that has a much pronounced variation between  $0^\circ/90^\circ$  and  $\pm 45^\circ$ . The polar plots are more representative and show the concordance between theoretical and experimental validation.

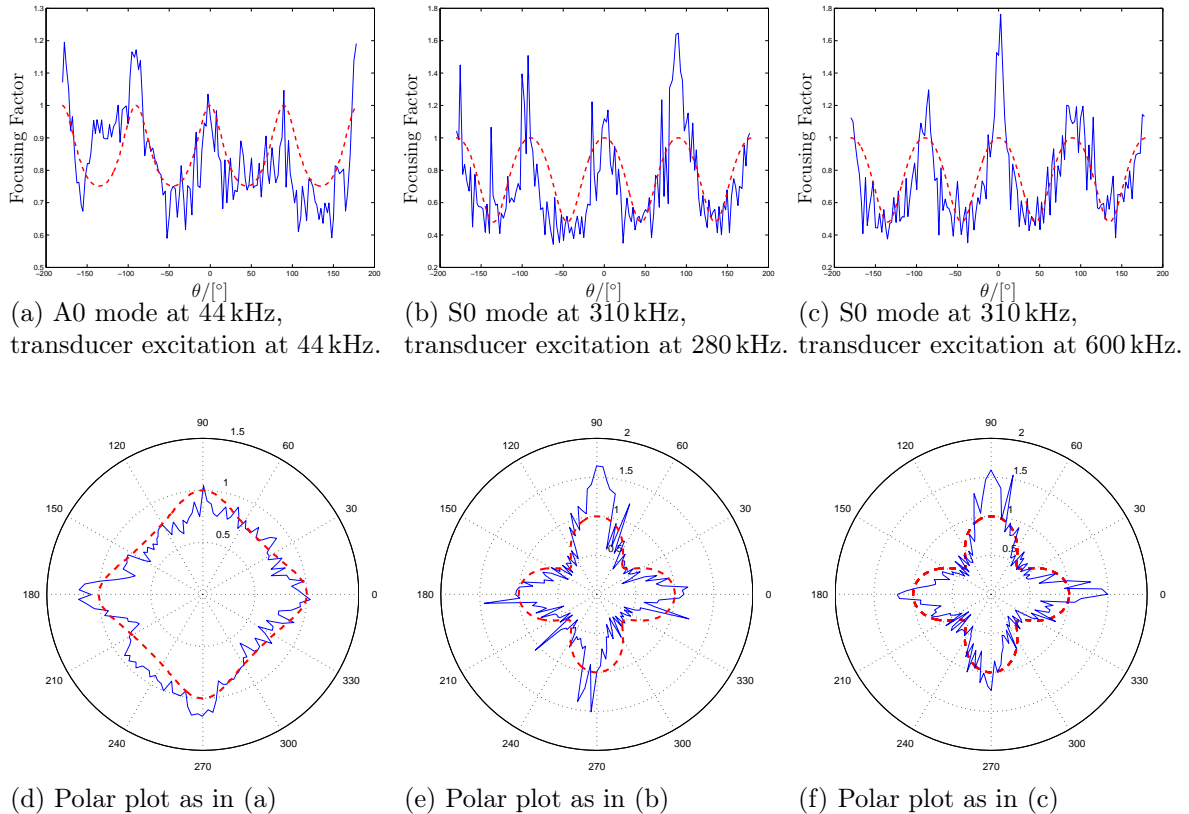


Figure 8: Focusing factor,  $\sqrt{A(\theta)}$ , for the A0 and S0 modes.

## 5. Conclusion

In this work, the effect of elastic focusing was studied and experimentally verified on a multilayer structural textile laminate. The profile of velocity group curves and the amplification of the wave amplitude as a function of the direction of propagation of the guided waves are theoretically calculated using the multilayered plate model, and these predictions agree with the experimental results. The curves show the effective anisotropic wave propagation character in the laminate. The theoretical predictions of the group velocities at 44 kHz, 66 kHz, 95 kHz and 310 kHz are in agreement with those observed in the experiments.

The A0 mode shows a smoother angular variation of the Maris factor, while the Maris factor for the S0 mode is much more directional for this plate layup. Theses results of mode dependent elastic focusing effect are similar to previous works [6] and must be taken into account to choose the adequate propagating mode in NDE or SHM applications, or

to force compensations of angular energy distribution of a wave mode.

## Acknowledgements

The authors wish to thank to the *CAPES Foundation, Ministry of Education of Brazil* and to the *Ministerio de Economía y Competitividad del Gobierno de España* (project FIS2013-46829-R) for partially support the work, and to the *Alltec Materiais Compostos* for preparing the laminate samples.

## References

1. B. Taylor, H. J. Maris, and C. Elbaum, “Phonon focusing in solids,” *Phys. Rev. Lett.*, vol. 23, pp. 416–419, Aug. 1969.
2. H. J. Maris, “Enhancement of heat pulses in crystals due to elastic anisotropy,” *The Journal of the Acoustical Society of America*, vol. 50, no. 3B, pp. 812–818, 1971.
3. J. Philip and K. Viswanathan, “Phonon focussing in crystals,” *Physics Letters A*, vol. 61, no. 1, pp. 61–62, 1977.
4. A. A. Kolomenskii and A. A. Maznev, “Phonon-focusing effect with laser-generated ultrasonic surface waves,” *Phys. Rev. B*, vol. 48, pp. 14 502–14 508, Nov. 1993.
5. A. A. Maznev and A. G. Every, “Focusing of acoustic modes in thin anisotropic plates,” *Acta Acustica*, vol. 3, pp. 387–391, 1995.
6. B. Chapuis, N. Terrien, and D. Royer, “Excitation and focusing of lamb waves in a multilayered anisotropic plate,” *The Journal of the Acoustical Society of America*, vol. 127, no. 1, pp. 198–203, 2010.
7. H. Fu, Z. Hou, J. Fu, and Y. Ma, “Elastic anisotropy and phonon focusing in nial: Atomic study,” *Intermetallics*, vol. 42, no. 0, pp. 156–164, 2013.
8. A. H. Nayfeh, *Wave Propagation in Layered Anisotropic Media: with Application to Composites*, ser. North-Holland Series in Applied Mathematics and Mechanics. Elsevier Science, 1995.
9. S. I. Rokhlin and L. Wang, “Stable recursive algorithm for elastic wave propagation in layered anisotropic media: Stiffness matrix method,” *The Journal of the Acoustical Society of America*, vol. 112, no. 3, pp. 822–834, 2002.
10. M. J. S. Lowe, “Matrix techniques for modeling ultrasonic waves in multilayered media,” *Ultrasonics, Ferroelectrics and Frequency Control, IEEE Transactions on*, vol. 42, no. 4, pp. 525–542, 1995.
11. E. L. Tan, “Stiffness matrix method with improved efficiency for elastic wave propagation in layered anisotropic media,” *The Journal of the Acoustical Society of America*, vol. 118, no. 6, pp. 3400–3403, 2005.
12. H. Cunfu, L. Hongye, L. Zenghua, and W. Bin, “The propagation of coupled lamb waves in multilayered arbitrary anisotropic composite laminates,” *Journal of Sound and Vibration*, vol. 332, no. 26, pp. 7243 – 7256, 2013.